JOURNAL OF MATERIALS SCIENCE **34** (1999) 2943–2947

Location of Cu^{2+} ions in some protoned Nasicon-type phosphates

I. TAOUFIK, M. HADDAD*
Laboratoire de Spectronomie Physique, Faculté des Sciences, BP 4010 Béni M'hamed, Meknès, Morocco
E-mail: mhaddad@fsmek.ac.ma

R. BROCHU
Laboratoire de Chimie du Solide et Inorganique Moléculaire, URA CNRS 1495, Groupe de Cristallochimie, Université de Rennes, Avenue du Général Leclerc, 35042 Rennes Cedex, France

R. BERGER
UMR Université Bordeaux-I, CNRS 5798, 351 cours de la Libération, 33405 Talence Cedex, France

Nasicon-type phosphates $Cu_{1-x}H_xZr_2(PO_4)_3$ ($0 < x < 1$) and $Cu_{1-x}H_{2x-1}Zr_2(PO_4)_3$ ($0.5 < x < 1$) have been investigated by magnetic susceptibility and electron paramagnetic resonance (EPR). Room-temperature EPR spectra at X-band (9.5 GHz) exhibit relatively different local information about paramagnetic environments in the two sets. Analysis by computer simulations of $Cu_{1-x}H_xZr_2(PO_4)_3$ spectra reveals that Cu^{2+} ion is located in an axially distorted octahedron, which can be assigned to the M(1) site. However, in the case of $Cu_{1-x}H_{2x-1}Zr_2(PO_4)_3$, EPR parameters suggest that Cu^{2+} ions are distributed in two types of sites with axial and lower than axial symmetries; these latter can be attributed to M(1) and M(2) sites respectively. *g* and *A* components are related to structural properties using molecular orbital method. Data are obtained on variations of the bond covalence with the composition.

1. Introduction

Nasicon-type phosphates have been extensively studied and they present various applications. In addition to their ionic conductivity they can be used as electrode materials, low thermal expansion ceramics, luminophores and catalysts [1–10]. Their ionic exchange properties interest the nuclear industry and they can help to store radioactive wastes [11].

The copper Nasicon-type phosphates are favored among other compounds by the presence of copper in two oxidization states (+1 and +2). These phosphates have been used as catalysts for oxidative dehydrogenation reactions [6–8]. $CuZr_2(PO_4)_3$ was lately discovered as the first Cu(I)-rich insulator phosphor exhibiting two types of emitting centers [9]; as the structure present a vacant character, the enrichment in these Cu(I) centers has been also performed [10]. Oxidation of $CuZr_2(PO_4)_3$ leads reversibly to the Nasicon phosphate $Cu_{0.5}Zr_2(PO_4)_3$ involving a redox system in a broad temperature range without three-dimensional network modification, since it displays a substantial rigidity [12]. Recent works using EPR experiment at X and Q bands of the $Cu_{0.5}Zr_2(PO_4)_3$ phosphate have revealed the presence of Cu^{2+} ion in both M(1) and M(2) sites of the Nasicon-structure [13]. Furthermore, Cu^{+}-H^{+} exchange has studied in $CuZr_2(PO_4)_3$, leading to new derived protoned phosphates as supports for catalysis [1, 2], formulated as follows: $Cu_{1-x}H_xZr_2(PO_4)_3$ ($0 < x < 1$) and $Cu_{1-x}H_{2x-1}Zr_2(PO_4)_3$ ($0.5 < x < 1$). These phosphates, being Cu(I) and Cu(II)-rich compounds respectively, have been investigated by different techniques (X-ray diffraction, Infrared spectroscopy, EXAFS, . . .) [1, 5]. They belong to Nasicon-type family with a three-dimensional network built up of ZrO_6 octahedra sharing corners with PO_4 tetrahedra (Fig. 1). Its structures show triclinic distortion compared with that of $NaZr_2(PO_4)_3$ [1], in which two sites usually labeled as M(1) and M(2) can be occupied by copper ions. The M(1) site is a trigonally distorted octahedron, formed by the common faces of two neighboring ZrO_6 octahedra perpendicular to the *c*-axis of the hexagonal cell. Thus the 3D-network can be considered as made up of infinite ribbons $[O_3ZrO_3M(1)O_3ZrO_3M(1)O_3ZrO_3]_\infty$ linked by PO_4 tetrahedra. The M(2) site with a coordination varying from eight to ten is located in a large and distorted cavity between these layers.

In the lack of detailed structural information concerning the distribution and the local environment

* To whom correspondence should be addressed.

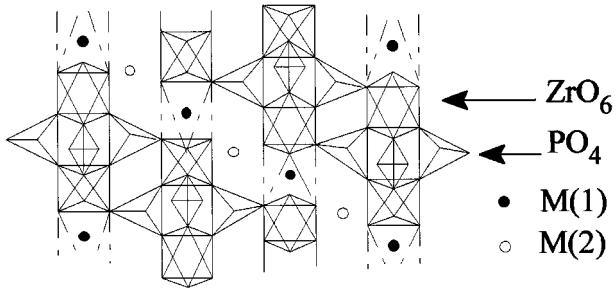

Figure 1 Chaining of ZrO_6 octahedra and PO_4 tetrahedra in Nasicon-type structure.

of Cu^{2+}, the $Cu_{1-x}H_xZr_2(PO_4)_3$ $(0 < x < 1)$ and $Cu_{1-x}H_{2x-1}Zr_2(PO_4)_3$ $(0.5 < x < 1)$ sets have been investigated using EPR spectroscopy and magnetic susceptibility measurements. Covalence of copper-oxygen bondings is discussed in terms of the Molecular Orbital theory in the case of $Cu_{1-x}H_{2x-1}Zr_2(PO_4)_3$.

2. Experimental

$Cu_{1-x}H_xZr_2(PO_4)_3$ samples $(0 < x < 1)$ were obtained by washing the compound $CuZr_2(PO_4)_3$ with 0.3N HCl. This latter compound was previously prepared by heating a stoichiometric mixture of ZrP_2O_7, ZrO_2 and Cu_2O. The oxidation of the products at 400 °C leads to $Cu_{1-x}H_{2x-1}Zr_2(PO_4)_3$ samples with $0.5 < x < 1$. The preparation mode has been described in Ref. [1].

EPR spectra were recorded at room temperature on Varian spectrometer operating at X-band frequency (9.5 GHz) using a dual sample cavity. It produces the first derivative of the absorption spectra with respect to the magnetic field B. The static magnetic field is measured by means of a nuclear flux-meter linked up to a Hewlett-Packard frequency counter; the microwave frequency is measured with the same counter.

Magnetic susceptibility measurements in the temperature range from 4.2 K to the ambient were carried out using the Faraday method.

3. Results

Figs 2 and 3 illustrate the room temperature EPR spectra recorded at X-band for $Cu_{1-x}H_xZr_2(PO_4)_3$ and $Cu_{1-x}H_{2x-1}Zr_2(PO_4)_3$ solid compounds respectively. Several compositions have been investigated $(1-x = 0.03;\ 0.24;\ 0.26$ for $Cu_{1-x}H_xZr_2(PO_4)_3$ and $1-x = 0.15;\ 0.20;\ 0.24;\ 0.26$ for $Cu_{1-x}H_{2x-1}Zr_2(PO_4)_3)$. Four hyperfine lines occur, they are attributed to the interaction between the unpaired electronic spin $(S = 1/2)$ and the nuclear one $(I = 3/2)$ of Cu^{2+} ion. For the first set this structure is relatively resolved, the hyperfine line intensities are low and slightly favored by the copper content. For the second one the spectra present greater width with poorly resolved hyperfine structure.

The spectra have been described by the spin Hamiltonian formed by the Zeeman term perturbed by the hyperfine one [13]:

$$H_s = \beta S g B + S A I, \qquad (1)$$

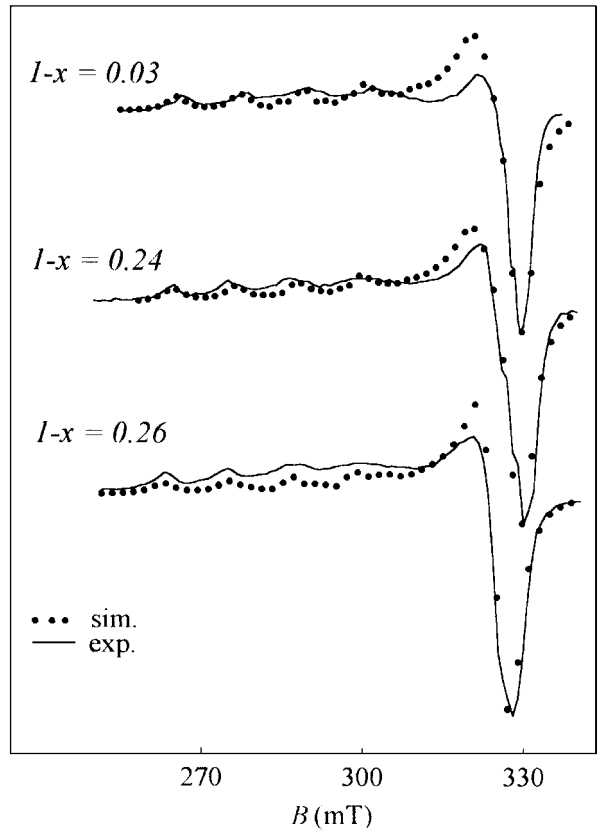

Figure 2 X-band EPR spectra of $Cu_{1-x}H_xZr_2(PO_4)_3$ compounds.

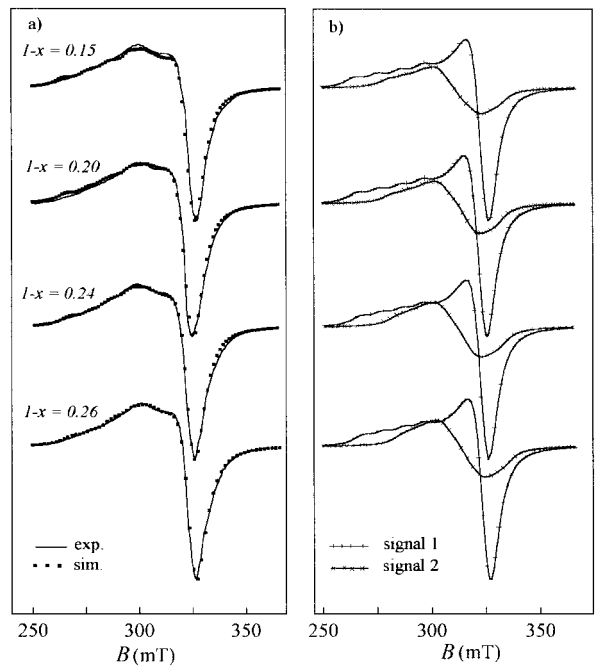

Figure 3 X-band EPR spectra of $Cu_{1-x}H_{2x-1}Zr_2(PO_4)_3$ compounds. (a) Experimental and computed spectra, (b) the components of its decomposition into signals 1 and 2.

where β is the Bohr magneton, B the static magnetic field, g and A the g-factor and the hyperfine term A tensors, respectively.

The resonance intensity is written as [13]:

$$I(B) = \sum_m \int_\theta \int_\varphi \overline{W}(\theta, \varphi) F((B - B_0)/\Delta B) \sin\theta \, d\theta \, d\varphi, \qquad (2)$$

TABLE I EPR parameters of $Cu_{1-x}H_xZr_2(PO_4)_3$ and $Cu_{1-x}H_{2x-1}Zr_2(PO_4)_3$ spectra

Compound	$1-x$		g_x	g_y	g_z	A_x (mT)	A_y (mT)	A_z (mT)	ΔB (mT)
$Cu_{1-x}H_xZr_2(PO_4)_3$	0.03		2.063	2.085	2.389	1.4	2.0	13.8	2.1
	0.24		2.064	2.086	2.394	1.2	2.0	14.0	2.45
	0.26		2.084	2.084	2.402	8.0	8.0	14.8	2.5
$Cu_{1-x}H_{2x-1}Zr_2(PO_4)_3$	0.15	Signal 1	2.093	2.093	2.410	2.2	1.4	12.6	5.3
		Signal 2	2.097	2.168	2.316	6.0	5.6	9.0	5.3
	0.20	Signal 1	2.089	2.090	2.408	1.4	1.5	12.0	5.4
		Signal 2	2.098	2.171	2.306	4.4	5.0	8.6	5.4
	0.24	Signal 1	2.092	2.093	2.400	1.0	1.3	11.4	5.5
		Signal 2	2.084	2.170	2.296	4.8	5.2	7.6	5.5
	0. 26	Signal 1	2.087	2.089	2.394	1.0	1.4	11.2	5.55
		Signal 2	2.077	2.156	2.283	5.2	5.4	7.0	5.55

$\overline{W}(\theta, \varphi)$ is the transition probability for the hyperfine line corresponding to a magnetic quantum number of spin m, it depends on the orientation of the applied static magnetic field with respect to the principal axes of the g-tensor. $F((B-B_0)/\Delta B)$ is the first derivative of the function-shape, B_0 the resonance magnetic field and ΔB the half-width at half-height. The spectra have been simulated using an isotropic line-width and more marked anisotropies of the g and A tensors.

The simulated spectra are compared with the experimental ones for $Cu_{1-x}H_xZr_2(PO_4)_3$ (Fig. 2); the hyperfine structure is reproduced in computing one signal. The EPR parameters derived from these fits are reported on Table I. As $Cu_{1-x}H_{2x-1}Zr_2(PO_4)_3$ compounds EPR spectra are very similar to that of $Cu_{0.5}Zr_2(PO_4)_3$ prepared by solid route (for which the presence of two EPR signals has been concluded using X and Q bands [13), computations in Fig. 3a are therefore realized for this second set taking into consideration two signals, called thereafter signal 1 and signal 2 (Fig. 3b). The signal 1 is similar to $Cu_{1-x}H_xZr_2(PO_4)_3$ EPR spectra with a partially resolved hyperfine structure, while the second one is not resolved. Best-fits simulation parameters are listed in Table I.

Fig. 4 shows the variation of the magnetic susceptibility inverse, relative to $Cu_{1-x}H_{2x-1}Zr_2(PO_4)_3$ compounds ($1-x=$ 0.26 and 0.20), versus temperature from 293 to 4 K. The curve $\chi_m^{-1}=f(T)$ is fitted to a straight line agreeing with the Curie's law.

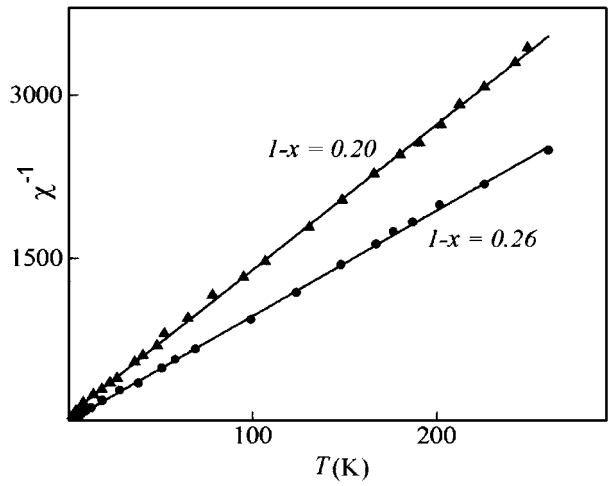

Figure 4 Inverse of magnetic susceptibility of $Cu_{1-x}H_{2x-1}Zr_2(PO_4)_3$ compounds versus temperature.

4. Discussion

4.1. EPR parameters and characterization of Cu^{2+} sites

$Cu_{1-x}H_xZr_2(PO_4)_3$ contains a very low Cu^{2+} content which lightly increases with $(1-x)$, the line-width ΔB growth (Table I) is explained by the decrease of the average distance between paramagnetic centers as their rates increase ($\Delta B \propto \langle r^{-3} \rangle$). A maximal anisotropy of g and A tensors is observed along the *local* z-axis, while anisotropy can be neglected in the perpendicular plane. So, the symmetry can be considered as quasi-axial and we can define parallel and perpendicular components with respect to the z-axis:

$$g_\parallel = g_z, \quad g_\perp = \frac{g_x + g_y}{2},$$

$$A_\parallel = A_z, \quad A_\perp = \frac{A_x + A_y}{2}.$$

g-factor values suggest a predominate $|d_{x^2-y^2}\rangle$ ground orbital state and an axially distorted octahedral oxygen environment of Cu^{2+} ion (as $g_\parallel > g_\perp > g_e$ with $g_e = 2.0023$ is the free-electron g-value [14–17]) which would be close to the M(1) site geometry.

In the case of $Cu_{1-x}H_{2x-1}Zr_2(PO_4)_3$ compounds the C Curie's constant [18], deduced from the magnetic susceptibility measurements (Fig. 4), allows to estimate the Cu^{2+} concentration (Table II); the rate of paramagnetic ions increases with the copper content.

As one can see from Table I, g-tensor is orthorhombic such as $g_z > g_y$, $g_x > g_e$; these values are typical of

TABLE II Estimated Cu^{2+} ion percentages in $Cu_{1-x}H_{2x-1}Zr_2(PO_4)_3$ deduced from magnetic susceptibility measurements

Total copper concentration $1-x$	Curie's constant (C)	Cu^{2+} concentration	Cu^{2+}/Cu_{total}%
0.26	0.104	0.21	81
0.20	0.075	0.15	75

TABLE III Axial γ and orthorhombic ρ distortion degrees in $Cu_{1-x}H_{2x-1}Zr_2(PO_4)_3$

Site	$1-x$	γ	ρ
M(1)	0.15	0.317	0.0
	0.20	0.310	0.003
	0.24	0.308	0.006
	0.26	0.306	0.012
M(2)	0.15	0.184	0.272
	0.20	0.176	0.320
	0.24	0.169	0.344
	0.26	0.167	0.345

Cu^{2+} ion in a distorted octahedron. The orthorhombic distortion degree is given by [19]:

$$\rho = \frac{g_y - g_x}{\gamma}, \tag{3}$$

with $\gamma = g_z - (g_y + g_x)/2$ being the degree of the axial distortion. Table III reports axial and orthorhombic distortion degrees calculated for the signals 1 and 2 of the simulated spectra. The increase of ρ in terms of $(1-x)$ indicates that the distortion is generally favored by Cu^{2+} ion density, in the same time the decreasing γ value suggests the Cu^{2+} octahedron shrinking; this can be linked to the fact that oxygen-shells electrostatic repulsion between two neighboring octahedra is expected to reduce as the number of Cu^{2+} ions increases [1]. According to the g-values of the signal 1 (Table I), we note that the Cu^{2+} ion environment is axially distorted. However, the large g-tensor anisotropy of the signal 2 (Table III) can be explained in terms of a highly distorted Cu^{2+} surrounding. The presence of the two constituent signals 1 and 2 shows that Cu^{2+} ions are distributed on two crystallographically non-equivalent sites. Similarly to $Cu_{0.5}Zr_2(PO_4)_3$ [13], these signals can be respectively attributed to Cu^{2+} ions in both M(1) and M(2) sites. The relative number of paramagnetic centers in each site determined by double integration of the corresponding EPR signal indicates that these sites are not equally occupied. Fig. 5 exhibits the evolution of the ratio of the Cu^{2+} occupation of M(2) sites to that of M(1) ones versus $(1-x)$. This shows that Cu^{2+} ions are located in majority at M(1) sites (from about 73% for $1-x=0.15$ to 69% for $1-x=0.26$), the M(2) sites are ready to be occupied as the copper content increases.

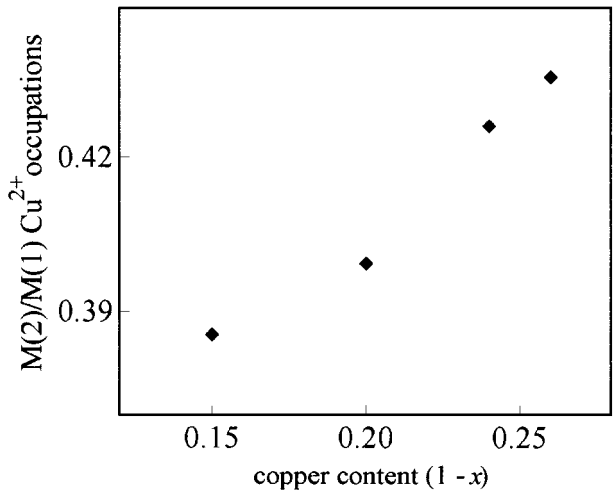

Figure 5 Evolution of the ratio of M(2) to M(1) Cu^{2+} occupations in $Cu_{1-x}H_{2x-1}Zr_2(PO_4)_3$ versus copper content.

4.2. Bond covalence

The spin hamiltonian parameters of the signals 1 and 2 vary with the composition of $Cu_{1-x}H_{2x-1}Zr_2(PO_4)_3$ set (Table I), this variation can be related to the covalent character of Cu^{2+} ion bondings in M(1) and M(2) sites.

In M(1) site Cu^{2+} ion is subjected approximately to axial crystalline field (e.g., D_{4h}). Using the relationships quoted in Ref. [20], we have calculated the molecular orbital coefficients α^2, β_1^2 and β^2 values, in terms of $g_\parallel$, $g_\perp$, $A_\parallel$ and $A_\perp$. These coefficients represent respectively the electron densities on $d_{x^2-y^2}$, d_{xy} and $d_{xz,yz}$ orbitals involved in Cu-O bondings, they describe respectively the covalence of in-plane σ and π bondings and out-of-plane π bondings. The calculations of these coefficients require the use of ΔE_{xy} and $\Delta E_{xz,yz}$ energy values, which correspond to $|d_{x^2-y^2}\rangle \rightarrow |d_{xy}\rangle$ and $|d_{x^2-y^2}\rangle \rightarrow |d_{xz,yz}\rangle$ electronic transitions respectively; the values 11300 and 14290 cm^{-1}, deduced from the $Cu_{0.5}Zr_2(PO_4)_3$ optical spectrum [13], have been adopted.

Results of calculations are listed in Table IV. α^2 change little in terms of the composition indicating that the local environment of Cu^{2+} ions is not largely affected. Furthermore, α^2 is close to 1 suggesting that the unpaired electron is almost located in the $d_{x^2-y^2}$ atomic orbital. Moreover, the slight decrease of α^2 as the copper content increases (Table IV) indicates that the Cu^{2+} ion σ bondings with the four equatorial oxygen become then more covalent. In the same way the $1-\beta_1^2$ coefficient decreases (Table IV) expressing therefore a more ionic character of in-plane π bondings. $(\alpha^2+\beta_1^2)/2$ characterizes the average d-electron delocalisation in xy plane of Cu^{2+} complex [21], as this parameter decreases the in-plane bondings become more covalent. This bonding parameter presents diminishing values when the rate of copper ion increases (Table IV). This variation signifies a "more free" unpaired electron in xy plane; consequently, the local directional difference γ between xy plane and z-axis (Table III) and the average g-factor g_{av} should decrease (Table IV). β^2 is close to 1 indicating that there is very low overlaps of d-orbitals with ligand p_z atomic orbitals in xz and yz planes; hence, the out-of-plane π bondings of the CuO_6 octahedron are ionic. This latter character is consistent

TABLE IV Molecular orbital coefficients and Cu^{2+} parameters in M(1) site for $Cu_{1-x}H_{2x-1}Zr_2(PO_4)_3$ compounds

$1-x$	α^2	$1-\beta_1^2$	β^2	$(\alpha^2+\beta_1^2)/2$	g_{av}
0.15	0.84	0.13	0.98	0.855	2.199
0.20	0.82	0.12	1.00	0.850	2.201
0.24	0.80	0.11	1.00	0.845	2.195
0.26	0.78	0.10	0.90	0.840	2.190

TABLE V The anisotropic hyperfine terms a_{dx}, a_{dy} and a_{dz}, the unpaired spin density α^2 and the average g-factor g_{av} of Cu^{2+} ions in M(2) sites of $Cu_{1-x}H_{2x-1}Zr_2(PO_4)_3$

$1-x$	a_{dx} (mT)	a_{dy} (mT)	a_{dz} (mT)	α^2	g_{av}
0.15	8.2	5.4	−13.6	0.66	2.194
0.20	7.3	5.2	−12.5	0.60	2.192
0.24	7.2	4.7	−11.9	0.57	2.183
0.26	7.0	4.6	−11.6	0.56	2.172

with the model of the square-planar configuration in which the electron density is approximately concentrated in the equatorial plane.

For the portion of Cu^{2+} ions occupying M(2) sites in $Cu_{1-x}H_{2x-1}Zr_2(PO_4)_3$ hosts the symmetry is lower than axial, the approximation of the square-planar model is not valid. For simplicity, we assume an orthorhombic symmetry (e.g., D_{2h}) [13]. Under the influence of this field the $|d_{x^2-y^2}\rangle$ ground orbital state is combined with the $|d_{z^2}\rangle$ excited orbital state [15]:

$$|\text{Ground state}\rangle = \alpha(|d_{x^2-y^2}\rangle - t|d_{z^2}\rangle), \qquad (4)$$

where α^2 is the probability of the electron to be found in metal d-orbitals, and t the mixing ratio of the d_{z^2} excited orbital to the $d_{x^2-y^2}$ orbital linked to g_x and g_y by the following relationship [15]:

$$\frac{(1-\sqrt{3}t)^2-(1+\sqrt{3}t)^2}{(1-\sqrt{3}t)^2+(1+\sqrt{3}t)^2} = \frac{\Delta g_x - \Delta g_y}{\Delta g_x + \Delta g_y}, \qquad (5)$$

with $\Delta g_{x,y} = g_{x,y} - g_e$. The values of the mixing ratio t of the d_{z^2} excited orbital to the $d_{x^2-y^2}$ orbital are not negligible, it ranges from 8 to 11%.

Using the relations quoted in Ref. [15] we have also calculated, in terms of EPR-parameters, the anisotropic hyperfine terms a_{d_i} ($i = x$, y and z) and the d-orbital unpaired spin density α^2 (Table V). For these ions the absolute values of a_{d_x}, a_{d_y}, a_{d_z} and α^2 decrease as copper ion rate increases (Table V). It suggests that the covalence become more important and the unpaired electron tends to move more far from the nucleus along the three x, y and z directions. This evolution can be explained by the increase of copper content which reduces the absolute value of the negative charge of ligand. In accordance with this result, the directional difference γ (Table III) and also g_{av} tend to decrease (Table V). The relatively smaller values of α^2 indicate that the in-plane $\sigma_{Cu\text{-}O}$ bondings in M(2) sites are more covalent than in M(1) ones.

5. Conclusion

The exchange Cu^+-H^+ reaction in the $CuZr_2(PO_4)_3$ host has formed two Nasicon-type sets with variable rates of copper. In $Cu_{1-x}H_xZr_2(PO_4)_3$ compounds, Cu^{2+} ion is located in axially distorted octahedron which concords with M(1) site geometry. The g-factor components suggest that the ground orbital state is predominately $|d_{x^2-y^2}\rangle$.

The EPR results reported in the case of $Cu_{1-x}H_{2x-1}Zr_2(PO_4)_3$ have revealed that Cu^{2+} ions are located in M(1) and M(2) sites, with a majority in the first one; the ratio of the Cu^{2+} occupation of M(2) sites to that of M(1) ones rises with copper content. Following the molecular orbital theory Cu^{2+} ion in M(1) site is interpreted by a model of square-planar configuration with a $|d_{x^2-y^2}\rangle$ predominant ground orbital state character. The g-factor components suggest a more distorted geometry of coordination in M(2) sites and the fundamental orbital state is $|d_{x^2-y^2}\rangle$ with a small admixture of the $|d_{z^2}\rangle$ excited orbital state. The in-plane $\sigma_{Cu\text{-}O}$ bondings in M(2) sites are more covalent than in M(1) ones.

References

1. R. BROCHU, A. LAMZIBRI, A. AADANE, S. ARSALANE and M. ZIYAD, *Eur. J. Solid State Inorg. Chem.* **28** (1991) 253.
2. A. SERGHINI, R. BROCHU, M. ZIYAD, M. LOUKAH and J. C. VEDRINE, *J. Chem. Soc. Faraday Trans.* **87** (1991) 2487.
3. R. BROCHU, M. EL-YACOUBI, M. LOUËR, A. SERGHINI, M. ALAMI and D. LOUËR, *Mater. Res. Bull.* **32** (1997) 15.
4. L. BENNOUNA, S. ARSALANE, R. BROCHU, M. R. LEE, J. CHASSAING and M. QUARTON, *J. Solid State Chem.* **114** (1995) 224.
5. A. EL-JAZOULI, *Adv. Mater. Res.* **1/2** (1994) 105.
6. E. FARGIN, I. BUSSEREAU, R. OLAZCUAGA, G. LE FLEM, C. CARTIER and H. DEXPERT, *J. Solid State Chem.* **112** (1994) 176.
7. A. SERGHINI, M. KACIMI, M. ZYIAD and R. BROCHU, *J. de Chimie Physique* **85** (1988) 499.
8. M. ZIYAD, R. AHMAMOUCH, M. ROUIMI, S. GHARBAGE and J. C. VEDRINE, *Solid State Ionics* **110** (1998) 311.
9. G. LE POLLES, C. PARENT, R. OLASCUAGA and G. LE FLEM, *C. R. Acad. Sci., Paris* **306** (1988) 765.
10. A. BOIREAU, J. L. SOUBEYROUX, P. GRAVEREAU, R. OLAZCUAGA and G. LE FLEM, *J. Alloys Compd.* **188** (1992) 113.
11. S. I. LIMAYE, D. K. AGRAWAL and H. A. MCKINSTRY, *Comm. Amer. Ceram. Soc.* **C232** (1987).
12. A. EL-JAZOULI, M. ALAMI, R. BROCHU, J. M. DANCE, G. LE FLEM and O. HAGENMULLER, *J. Solid State Chem.* **71** (1987) 444.
13. I. TAOUFIK, M. HADDAD, A. NADIRI, R. BROCHU and R. BERGER, *J. Phys. Chem. Solids* (1999) in press.
14. D. L. GRISCOM, *J. Non-Cryst. Solids* **40** (1980) 211.
15. P. CHAND, G. C. UPRETI, M. UMAR and R. J. SINGH, *Phys. Status Solidi B* **131** (1985) 357.
16. J. L. RAO, V. PADMAVATHI, K. V. NARASIMHULU and Y. NAGARAJA NAIDU, *Spectrochimica Acta* **51** (1995) 2531.
17. L. D. BOGOMOLOVA, YU. G. TEPLIAKOV and F. CACCAVALE, *J. Non-Cryst. Solids* **194** (1996) 291.
18. M. QUARTON and M. T. OUMBA, *Mater. Res. Bull.* **18** (1983) 967.
19. A. BALS and J. KLIAVA, *J. Phys. Cond. Matter* **3** (1991) 6209.
20. D. KIVELSON and R. NEIMAN, *J. Chem. Phys.* **35** (1961) 149.
21. I. SIEGEL and E. P. JONES, *ibid.* **57** (1972) 2364.

Received 28 July 1997
and accepted 15 December 1998